

ARTICLES

Near-threshold proton-induced neutral pion production from deuterium

M. A. Pickar

Department of Physics & Astronomy, University of Kentucky, Lexington, Kentucky 40506

A. D. Bacher, H. O. Meyer, and R. E. Pollock

Department of Physics, Indiana University, and Indiana University Cyclotron Facility, Bloomington, Indiana 47405

G. T. Emery

Physics Department, Bowdoin College, Brunswick, Maine 04011

(Received 21 November 1991)

Total cross sections and angular distributions for the differential cross section and analyzing power of the reaction ${}^2\text{H}(\vec{p}, \pi^0){}^3\text{He}$ have been measured at four energies very near threshold ($0.1 < T_{\pi}^{\text{c.m.}} < 2.7$ MeV). The large asymmetries observed in the angular distributions of the differential cross section indicate strong constructive interference between the amplitudes for s -wave pion emission and the amplitudes for p -wave emission. A measure of the s -wave strength at zero energy is obtained and found to be consistent with the results from pionic atoms. The new data indicate that the excitation function for this reaction differs significantly from that of $p + n \rightarrow d + \pi^0$.

PACS number(s): 25.40.Qa, 25.10.+s

I. INTRODUCTION

The process of nucleon-induced pion production, or (N, π) , has long been of interest because it is one that intrinsically involves a large momentum transfer to the target nucleus ($q > 500$ MeV/ c). An increased understanding of this process should add to our understanding of processes involving high momentum transfer in general, and thus lead to a better description of the short range interaction between nucleons within a nucleus.

The determination of the reaction mechanism for (N, π) is complicated by the fact that a general description of the mechanism must include many terms. One is in general forced to make assumptions that lead to the neglect of all but a few of these terms. The results of such studies are made further ambiguous by uncertainties in the short range behavior of nuclear wave functions. Investigations of mechanisms for (N, π) are perhaps best served by restricting oneself to those physical circumstances that clearly isolate one aspect of the process and that minimize uncertainties arising from nuclear wave functions.

It is possible to group the mechanisms for (N, π) into two categories: "resonant" and "nonresonant" terms. The "resonant" production mechanisms are those in which two nucleons make a transition to an intermediate state consisting of a $\Delta(J^{\pi} = \frac{3}{2}^{+}, I = \frac{3}{2})$ coupled to a nucleon, which then decays into a pion and two nucleons ($NN \rightarrow N\Delta \rightarrow NN\pi$). These are expected to dominate at pion energies of ~ 120 MeV. As the width of a "free" Δ is 120 MeV, one must go to low energy to reach a kinematic region in which those mechanisms that are "non-

resonant" will become dominant and unambiguous.

This work describes an experimental study of ${}^2\text{H}(p, \pi^0){}^3\text{He}$ that is *extremely* close to threshold ($0.1 < T_{\pi}^{\text{c.m.}} < 2.7$ MeV). As such it provides an effective means of investigating nonresonant production mechanisms. Because the initial and final state nuclear wave functions for this reaction are better understood than those of other nuclei, the problems induced by uncertainties in nuclear structure are reduced to minimal levels. Further, this reaction involves the *simplest* multinucleon system available, and thereby serves effectively as a laboratory for multinucleon studies, providing a bridge between our understanding of the fundamental process, $NN \rightarrow NN\pi$, and pion production from a heavy nucleus.

There have been a great number of experimental studies of the reaction ${}^2\text{H}(p, \pi^0){}^3\text{He}$, or its analog, over a wide range of energies. However, for $T_{\pi} < 4$ MeV the only cross section data that exist are those provided by pionic atoms. Thus it is hoped that the results provided by this experiment will prove useful in supplying information needed to understand the mechanics of pion production in the threshold region.

II. EXPERIMENTAL METHOD

This experiment was performed at the Indiana University Cyclotron Facility (IUCF). The measurements were made using a polarized proton beam incident on deuterated polyethylene (CD_2) foils at four laboratory energies, indicated in Fig. 1, corresponding to pion center-of-mass (c.m.) energies ($T_{\pi}^{\text{c.m.}}$) ranging from 0.11 to 2.68 MeV. The threshold energy for this reaction is 198.72 MeV.

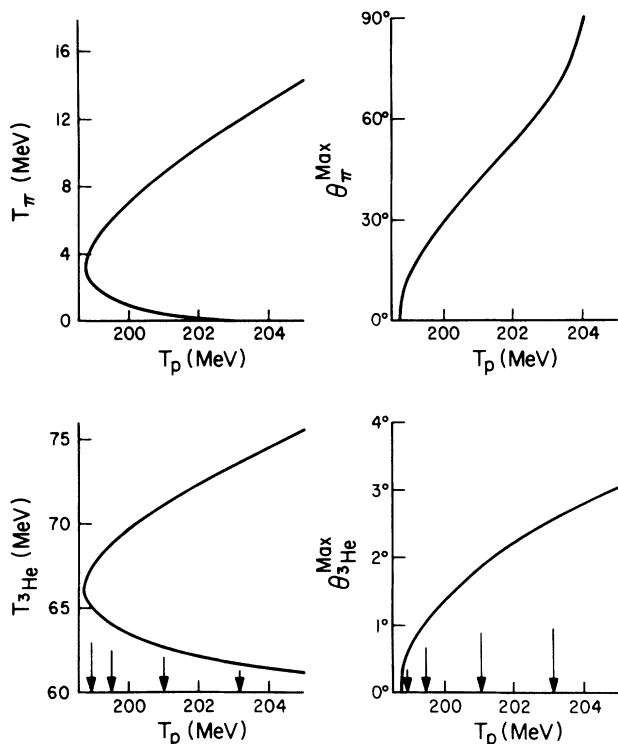


FIG. 1. The near-threshold kinematics for ${}^2\text{H}(p, \pi^0){}^3\text{He}$. The beam energies at which measurements were made are indicated by the arrows. The threshold for π^0 production is 198.72 MeV.

In this region very near threshold, the recoiling ${}^3\text{He}$ emerge with angles less than 3° and kinetic energies ranging from 61 to 74 MeV (see Fig. 1). They were momentum analyzed using the quadrupole-dipole-dipole-multipole (QDDM) spectrometer [1–3] positioned near zero degrees (Fig. 2). The intrinsic momentum resolution of this device ($\Delta p/p < 4 \times 10^{-4}$) is more than sufficient to permit a detailed determination of the angular distribution of the differential cross section for the $pd \rightarrow {}^3\text{He}\pi^0$ reaction through the measured distribution in energy of the recoils. The moderate angular acceptance of the QDDM (~ 3.4 msr) provides a high efficiency for collecting the recoils associated with the reaction because of their small range of emission angles in the laboratory (Fig. 1).

With the spectrometer in the near zero degree position, the beam was required to pass unobstructed between the slits defining the solid angle of the spectrometer. As a result, the range of angles accessible was 1.7° to the left and 3.2° to the right. This effectively limited complete investigations of this reaction by this method to proton energies less than ~ 204 MeV.

The proton beam stopped in a copper Faraday cup within the dipole magnet of the spectrometer, as indicated in Fig. 2. A large charged-particle flux at the focal plane originating from the beam striking this cup necessitated the construction of a focal plane detector capable of handling high rates. This device consisted of NE102 plastic scintillator hodoscope elements in three planes; ΔE (1.6 mm thick) and E (3.2 mm thick) planes for parti-

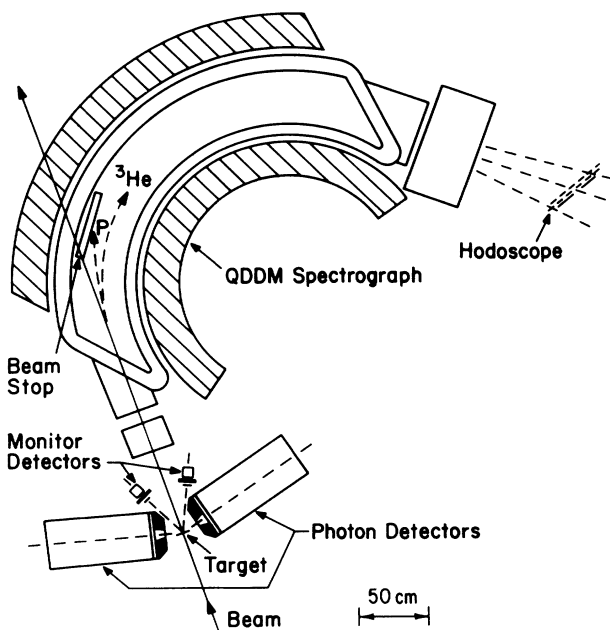


FIG. 2. A sketch illustrating the principal features of the experimental setup. The incident proton beam passes through a deuterated polyethylene foil target into a magnetic spectrograph (QDDM), where it finally impinges on an extended internal Faraday cup (beam stop). The recoiling ${}^3\text{He}$ are analyzed by the QDDM, and are identified in a hodoscope made of plastic scintillator. Coincident photons from the decay of the associated π^0 are detected in the arrays of lead glass photon detectors placed symmetrically about the target. Beam intensity and deuterium content of the target are monitored continuously with a pair of detectors placed symmetrically at small angles (monitor detectors).

cle identification, and a veto (2.4 mm thick) plane. There were six elements in each of the ΔE and E planes. These planes were half-overlapping so as to provide 11 coincident bins across the focal plane, each with a width equivalent to less than 400 keV in the recoil energy.

A coincidence between the ${}^3\text{He}$ particles and the decay gamma rays from the associated neutral pions was required to reject ${}^3\text{He}$ produced by the $(p, {}^3\text{He})X$ reaction in the carbon of the CD_2 target and particles produced in the beam stop. The mean life of the π^0 is very short ($\sim 10^{-16}$ s) and its principal decay mode is into two high energy photons ($\pi^0 \rightarrow \gamma\gamma$, 98.5%, and $E_\gamma = m_\pi c^2/2 = 68$ MeV for a π^0 at rest). Thus, our event signature consisted of a recoil ${}^3\text{He}$ in coincidence with either one or two prompt high energy photons from the target. A photon detector was positioned at 75° on each side of the target. The geometric solid angle of each detector (312 msr) was defined by a 7.62 cm thick lead collimator. Each photon detector consisted of an assembly of four lead glass Čerenkov detectors, each $15 \times 15 \times 30$ cm³ with a 12.7 cm diameter phototube on the rear face, yielding a cubic counter, $30 \times 30 \times 30$ cm³. The intrinsic efficiency of these detectors for the photons associated with the decay of the neutral pions in this study was $99 \pm 1\%$ [4]. With the photon detectors and spectrometer positioned as de-

scribed, it was impossible to obtain a ${}^3\text{He}-\gamma$ coincidence from the background reaction, $pd \rightarrow {}^3\text{He}\gamma$, by any direct means.

During the experiment, data were recorded event by event on magnetic tape. Information recorded included ΔE and E pulse heights, pulse heights in the photon counters, coincident bin in the hodoscope, photon detectors triggered, recoil time of flight (TOF) relative to the cyclotron rf, photon time of flight relative to the cyclotron rf, recoil time of flight relative to a photon trigger, and $\Delta E-E$ time of flight. Given all these parameters it was possible to make a very clean identification of the events of interest.

Figure 3 illustrates a typical two-dimensional rf- γ time-of-flight spectrum obtained with only the required hardware coincidence conditions. The γ_R and γ_L "singles" events are observed to be well above the background. The $\gamma_L\gamma_R$ "coincident" events have a much lower level of background.

With the cuts applied during off-line analysis the background drops to near negligible levels. Studies performed using natural carbon targets lead us to estimate a background contamination of less than 1% for any of the experimental configurations in the study.

Figure 4 illustrates a typical spectrum resulting from such an analysis. The parameters of interest at this stage of the analysis are the hodoscope bin, corresponding to recoil momentum, and the time of flight relative to the cyclotron rf. In this figure, recoil momentum decreases as hodoscope bin increases, i.e., bin 6 corresponds to the lowest energy recoils, associated with π^0 's emitted at 0° in the c.m., whereas decreasing bin numbers are associated with π^0 's emitted at larger and larger polar angles in the c.m. The recoil TOF is a relevant parameter because the path length in the magnet varies nearly linearly with the projected horizontal angle at which the recoils enter the

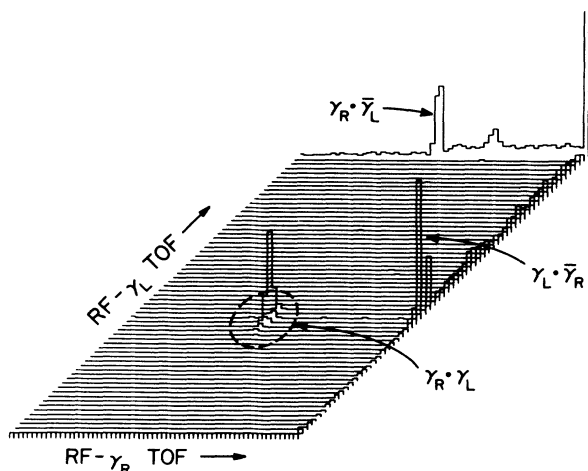


FIG. 3. A representative photon TOF (time-of-flight) spectrum, with only the cuts applied in hardware, for the left (γ_L) and right (γ_R) photon detectors. These data were taken at $T_p = 203.14$ MeV, with the apparatus adjusted to be sensitive to π^0 's emitted between 20° and 65° in the center of mass (c.m.). Note the three peaks associated with the three independent coincidence conditions: $\gamma_R\gamma_L$, $\bar{\gamma}_R\bar{\gamma}_L$, and $\gamma_R\bar{\gamma}_L$. The time calibration is 1.5 ns/channel.

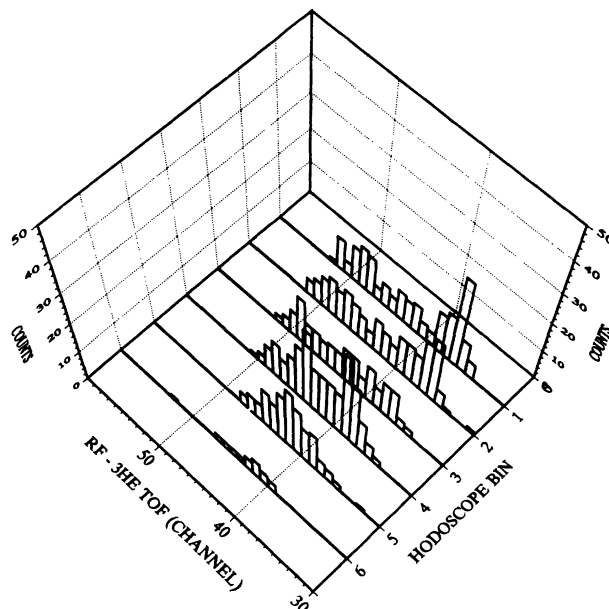


FIG. 4. A representative recoil spectrum. These data were obtained at $T_p = 199.48$ MeV, yielding π^0 's of 0.46 MeV in the center of mass (c.m.), with the apparatus set up to detect events associated with π^0 's emitted between 0° and 76° in the cm. Angles are decreasing in increasing hodoscope bin number. The rf- ${}^3\text{He}$ TOF is directly related to the projected horizontal angle at which the recoils enter the spectrometer. Each hodoscope bin has a width of ~ 0.40 MeV in energy. The time calibration for the recoil TOF is 0.37 ns/channel.

spectrometer. This information permits a determination of the left-right asymmetry, and thus of the angular distribution of the analyzing power, $A_y(\theta)$, where it was not possible to isolate a particular "side" by moving the spectrometer or its slits.

The end result of the data reduction was a set of yields for each hodoscope bin at each spectrometer field and angle setting, for each incident beam energy. These yields were the input for the data analysis, whose description follows.

III. DATA REDUCTION AND ANALYSIS

The extraction of angular distributions of cross sections and analyzing powers from the coincident spectra required a fitting procedure that incorporated corrections arising from instrumental effects. In this experiment the principal effects were sufficiently small and sufficiently understood as to incur relatively small systematic uncertainties in the final results. These corrections and the fitting procedures are described in what follows.

A. Corrections

1. Differential energy loss of the recoils

The angular distributions were reconstructed through a determination of the distribution in energy of the recoil

^3He . Effects that significantly distorted that spectrum had to be explicitly incorporated into the analysis. Chief among these was the differential energy loss of the recoil ^3He exiting the target. Although the targets were fairly thin (4 mg/cm² for the three lowest beam energies, and 11 mg/cm² for the highest beam energy), the maximum possible energy loss of the recoils in the targets was not negligible compared to the spread in energy of the recoils (see Fig. 1). One obtains a maximum energy loss of about 0.4 MeV for the thin target, and about 1.2 MeV for the thick target. This is to be compared to a kinematic dispersion of recoil energies of 3 MeV at the lowest bombarding energy studied, and a kinematic dispersion of 12 MeV at the highest energy.

2. Efficiency of the photon detectors

The intrinsic efficiency of the lead glass photon detectors for detecting the 55–75 MeV gamma rays associated with the decay in flight of the neutral pions produced in this measurement was unity to within 1% [4]. However, the probability for detecting one or both of the gamma rays associated with a specific recoil ^3He was considerably less, and was a function of experimental geometry, bombarding beam energy, and the associated pion direction. These probability functions were computed using Monte Carlo techniques over a grid in bombarding energy, T_p , and pion center-of-mass angles, $\cos\theta_{\pi}^{\text{c.m.}}$ and $\phi_{\pi}^{\text{c.m.}}$, sufficiently fine and with sufficient precision to incur no more than a 2% uncertainty in the analysis.

The three photon detector coincidence conditions possible in the hardware (γ_L , γ_R , and $\gamma_L\gamma_R$) had significantly different efficiencies. As we accumulated data with all three coincidence conditions simultaneously, this permitted an effective test of consistency on the analysis.

In order to perform an analysis using all the data it was necessary to compute the probability functions associated with the coincidence conditions $\gamma_L\bar{\gamma}_R$ and $\bar{\gamma}_L\gamma_R$. This permitted a fit to the data as a whole by breaking the yields up into the three independent sets $\{\gamma_L\gamma_R\}$, $\{\gamma_L\bar{\gamma}_R\}$, and $\{\bar{\gamma}_L\gamma_R\}$, which could then be fit simultaneously.

3. Edge effects of the photon collimators

There is an effective increase in the solid angle of the photon detectors due to photons that interact with the collimators near the edges of the defining apertures. Some of the flux from the resulting electromagnetic cascade can escape from the collimator edge to enter and trigger the photon detector, leading to a small, but significant, increase in the effective solid angle. Calculations were performed that demonstrated, for small increases in the solid angle, the π^0 detection efficiency varied linearly. Hence, the correction influenced only the absolute normalization. Monte Carlo calculations performed to calculate the effect yielded a $15\pm 3\%$ increase in the effective solid angle.

4. Finite angular acceptance

A preliminary analysis [5] gave evidence for forward peaking in the cross section. As each hodoscope bin was sensitive to an extended region of the phase space for the reaction, it was necessary to take into account the variation of the cross section in that region. This was done by assuming the cross sections and analyzing powers are reasonably well represented by Legendre expansions, i.e.,

$$\frac{d\sigma}{d\Omega} = \sum_{l=0}^{N_L} a_l P_l(x) \quad (1)$$

and

$$A_y \frac{d\sigma}{d\Omega} = \sum_{l=1}^{N_L} b_l P_l^1(x) \quad (2)$$

using the Legendre functions as given by Abramowitz and Stegun [6]. The coefficients a_l and b_l are to be obtained by fitting to the observed yields. One expects $N_L \leq 2$ in this very near threshold region, due to the suppression of higher order terms by penetrability factors associated with angular momentum ($kR \leq 0.2$ in this experiment). This assumption was tested in the final analysis.

5. Beam energy spread

The incident proton beam was not monoenergetic, typically having a width of 0.2 MeV (FWHM). Because the Legendre coefficients are expected to vary with energy, it is necessary to make provisions for that effect very near threshold. The momentum dependence of the coefficients in the vicinity of the centroid of the beam energy distribution, T_{cent} , was fixed to

$$a_l \propto p_{\pi}^{l+1}, \quad (3)$$

$$b_l \propto p_{\pi}^{l+1} \quad (4)$$

(where p_{π} is the pion momentum in the center of mass), as the result of a preliminary analysis, and also because this is the expected variation if “phase space” dominates the momentum dependence of the coefficients. The function describing the incident beam energy distribution, $P(T_p, T_{\text{cent}}, \text{FWHM})$, was well represented by a Gaussian at all but the lowest energy investigated, for which a directly measured distribution was used.

6. Other effects

Other effects studied included angular divergence of the beam due to its emittance and to multiple scattering in the target; multiple scattering of the recoils; energy straggling of the beam and the recoils; and absorption in a thin aluminum plate placed before the photon detectors. The corrections for these effects were small compared to those described in the previous sections.

B. Fitting the data

If one considers only the effects described in Secs. III A 1–III A 3 above, one may relate the observed yields

for a given hodoscope bin to the cross section in the center of mass, $d\sigma/d\Omega$, and to the analyzing power, A_y , by

$$Y_{\uparrow} = \int_{\Delta\Omega} d\Omega \frac{d\sigma}{d\Omega} (1 + P_{\uparrow} A_y \sin\phi) f_0 f_1 g, \quad (5)$$

$$Y_{\downarrow} = \int_{\Delta\Omega} d\Omega \frac{d\sigma}{d\Omega} (1 - P_{\downarrow} A_y \sin\phi) f_0 f_1 g. \quad (6)$$

The quantity $Y_{\uparrow(\downarrow)}$ is the observed yield with proton spin up (down); $P_{\uparrow(\downarrow)}$ is the polarization for spin up (down) incident protons; $\Delta\Omega$ is that region in the center of mass (c.m.) to which the hodoscope bin is sensitive; x is $\cos\theta_{\pi}^{\text{c.m.}}$; and ϕ is the azimuthal angle of the π^0 in the c.m.

The function $f_0(T_p, \Delta T, T_0, \Delta T_0; x, \phi)$ is the probability a recoil produced by a proton with energy T_p , from a target with a width ΔT associated with the energy loss of the recoils, detected in a hodoscope bin with centroid T_0 and width ΔT_0 , is associated with an event defined by π^0 cm coordinates (x, ϕ) . The function $f_1(T_p, x, \phi; \Omega)$ is the probability a recoil associated with an event defined by coordinates T_p , x , and ϕ passes through the slits defining a solid angle Ω . The function $g(T_p, x, \phi)$ is the probability one (or both) photon detectors trigger given an event with coordinates T_p , x , and ϕ .

It is more convenient to work with the reduced yields Y and ΔY , defined by

$$Y = \int_{\Delta\Omega} d\Omega \frac{d\sigma}{d\Omega} f_0 f_1 g \quad (7)$$

and

$$\Delta Y = \int_{\Delta\Omega} A_y \frac{d\sigma}{d\Omega} \sin\phi f_0 f_1 g. \quad (8)$$

If $d\sigma/d\Omega$ and $A_y d\sigma/d\Omega$ are sufficiently slowly varying in the angular region sampled by a given hodoscope bin, mean values can be readily obtained by removing these

functions from the integrals in (7) and (8) and dividing the measured yields by the remaining integrals over the various efficiency factors. This procedure was used to produce the preliminary results of [5].

In the final analysis the finite angular acceptance, the spread in the beam energy, the energy dependence of the observables, and the other effects outlined previously were incorporated. The yields may now be written as

$$Y = \sum_{l=0}^{N_L} a_l(T_{\text{cent}}) \int_{-\infty}^{\infty} dT_p P(T_p, T_{\text{cent}}, \text{FWHM}) \times [p_{\pi}(T_p)/p_{\pi}(T_{\text{cent}})]^{l+1} \times \int_{\Delta\Omega} d\Omega P_l(x) f_0 f_1 g \quad (9)$$

and

$$\Delta Y = \sum_{l=1}^{N_L} b_l(T_{\text{cent}}) \int_{-\infty}^{\infty} dT_p P(T_p, T_{\text{cent}}, \text{FWHM}) \times [p_{\pi}(T_p)/p_{\pi}(T_{\text{cent}})]^{l+1} \times \int_{\Delta\Omega} d\Omega P_l^1(x) f_0 f_1 g. \quad (10)$$

In each of the above two expressions everything within the integrals is a known quantity. We can therefore rewrite the above expressions more simply in terms of effective efficiency factors, as

$$Y \equiv \sum_{l=0}^{N_L} a_l(T_{\text{cent}}) \varepsilon_l(T_{\text{cent}}) \quad (11)$$

and

$$\Delta Y \equiv \sum_{l=1}^{N_L} b_l(T_{\text{cent}}) \varepsilon_l^*(T_{\text{cent}}). \quad (12)$$

We have such expressions for each hodoscope bin and detector geometry used at a given beam energy. These may be combined to define a pair of χ^2 ,

$$\chi_a^2 = \frac{1}{(N_{\text{data}} - N_L)} \sum_{i=1}^{N_{\text{data}}} \left[\left(Y_i - \sum_{l=0}^{N_L} a_l(T_{\text{cent}}) \varepsilon_{il}(T_{\text{cent}}) \right) / \delta Y_i \right]^2, \quad (13)$$

and

$$\chi_b^2 = \frac{1}{(N_{\text{data}} - N_L)} \sum_{i=1}^{N_{\text{data}}} \left[\left(\Delta Y_i - \sum_{l=1}^{N_L} b_l(T_{\text{cent}}) \varepsilon_{il}^*(T_{\text{cent}}) \right) / \delta \Delta Y_i \right]^2. \quad (14)$$

The Legendre coefficients, a_l and b_l , and the beam energy centroids, T_{cent} , were obtained by minimizing these χ^2 . The beam energy centroid was made a free parameter in the fitting procedure as it was a very important variable in the analysis and was not determined with sufficient precision by previous energy calibrations of the beam analysis system. The reaction itself provides sufficient sensitivity at the lowest energies to determine the beam energy centroid to within ± 50 keV.

In Fig. 5 the end result of the fit to the data obtained at a bombarding energy of 201.06 MeV is compared to the

yields at the two extremes of the recoil spectrum. These portions of the spectrum are those most sensitive to variations in the beam energy and to the corrections discussed in this section. The quality of the fits obtained is clearly illustrated.

IV. RESULTS

Tables I and II list the results of a representative analysis at one beam energy, $T_p = 199.48$ MeV ($T_{\pi}^{\text{c.m.}} = 0.46$ MeV). Table I, obtained using only the γ_L

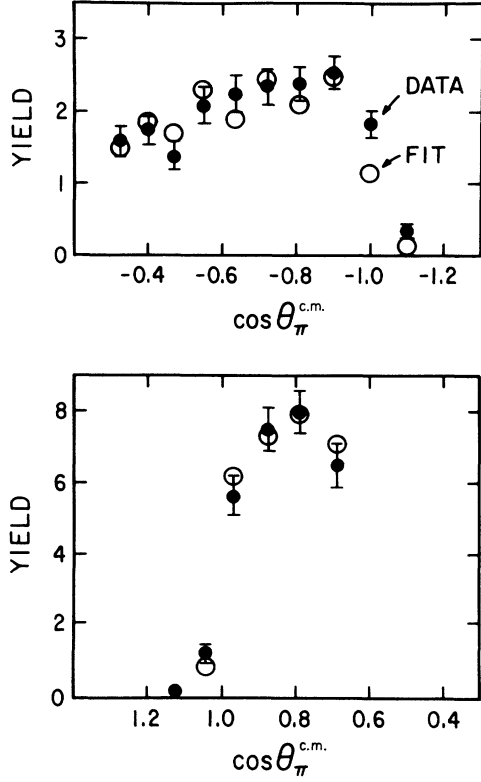


FIG. 5. Illustration of the quality of the fits obtained. The solid points are reduced yields obtained at a bombarding energy of 201.06 MeV. The error bars represent the statistical uncertainty. The open circles are the results of the fit. The results are plotted as a function of the mean value of the $\cos\theta_{\pi}^{c.m.}$ for the given hodoscope bin, as obtained from the mean energy of the recoils accepted by that bin. There is a simple linear relationship between the energy of a recoil and $\cos\theta_{\pi}^{c.m.}$. One obtains valid events outside of the region $-1 \leq \cos\theta_{\pi}^{c.m.} \leq 1$ because of distortions in the measured energy spectrum, caused primarily by differential energy loss in the target.

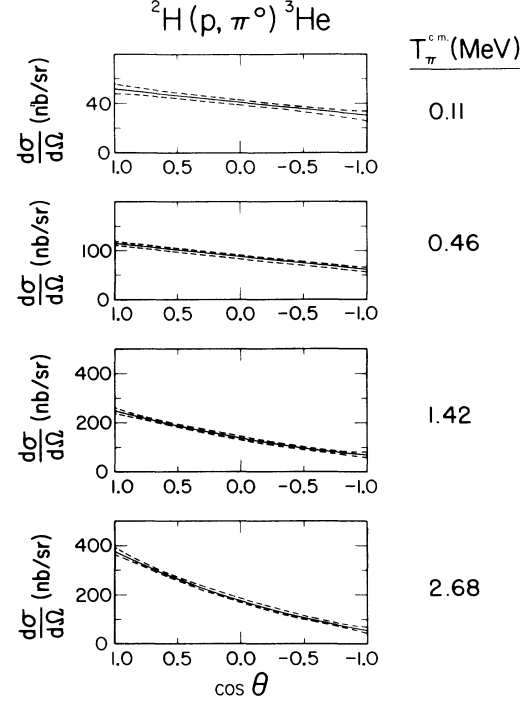


FIG. 6. Illustration of the differential cross sections resulting from the full analysis. The dashed lines indicate the one sigma bounds of uncertainty.

coincidence condition, demonstrates that there is sufficient sensitivity to the beam energy centroid to allow one to extract it to within ± 40 keV. From the table it is also evident that a_0 and a_1 are *essential* to a fit of the data. This was true at all energies studied. In this representative case, there is only marginal evidence for a significant contribution by a_2 . At the two higher energies there is increasing evidence for a non-negligible contribu-

TABLE I. Sample fits with coincidence condition γ_L at one energy ($T_p = 199.48$ MeV, $T_{\pi}^{c.m.} = 0.46$ MeV), illustrating the sensitivity of the analysis to T_{cent} , the centroid of the incident beam energy distribution, and to the coefficients a_0 , a_1 , and a_2 . The total number of π^0 , N_{π} , in this data set is 4636, and the total number of independent hodoscope bin measurements, N_{data} , is 28.

| T_{cent} (MeV) | N_L | χ^2 | a_0 (nb/sr) | a_1 (nb/sr) | a_2 (nb/sr) |
|---------------------|-------|----------|------------------|------------------|------------------|
| 199.38 | 0 | 7.77 | 84.8 ± 1.4 | | |
| 199.48 | 0 | 4.91 | 88.2 ± 1.5 | | |
| 199.58 | 0 | 16.90 | 81.4 ± 1.4 | | |
| 199.38 | 1 | 5.82 | 84.0 ± 1.4 | 21.4 ± 2.8 | |
| 199.45 | 1 | 2.49 | 87.3 ± 1.4 | 24.3 ± 2.8 | |
| 199.48 | 1 | 1.79 | 88.1 ± 1.4 | 25.8 ± 2.8 | |
| 199.51 | 1 | 2.40 | 87.7 ± 1.4 | 28.0 ± 2.8 | |
| 199.58 | 1 | 9.14 | 84.0 ± 1.4 | 34.4 ± 2.8 | |
| 199.38 | 2 | 4.12 | 87.4 ± 1.5 | 22.9 ± 2.8 | 27.7 ± 4.0 |
| 199.45 | 2 | 1.81 | 88.9 ± 1.5 | 25.6 ± 2.8 | 16.8 ± 3.8 |
| 199.48 | 2 | 1.58 | 88.9 ± 1.5 | 26.8 ± 2.8 | $+9.7 \pm 3.7$ |
| 199.51 | 2 | 2.49 | 87.8 ± 1.5 | 27.9 ± 2.8 | -0.9 ± 3.5 |
| 199.58 | 2 | 5.80 | 84.6 ± 1.4 | 28.4 ± 2.4 | -28.2 ± 2.9 |

TABLE II. Representative fits at one energy ($T_{\pi}^{c.m.} = 0.46$ MeV) for different coincidence conditions.

| Parameter | Coincidence condition | | | Full fit |
|-------------------|-----------------------|----------------|--------------------|----------------|
| | γ_L | γ_R | $\gamma_L\gamma_R$ | |
| N_{π} | 4636 | 4498 | 3107 | 6027 |
| N_{data} | 28 | 28 | 28 | 84 |
| $N_L = 0$ | | | | |
| χ^2 | 4.91 | 5.24 | 3.69 | 2.76 |
| a_0 (nb/sr) | 88.2 ± 1.5 | 90.6 ± 1.5 | 94.5 ± 1.8 | 85.9 ± 1.2 |
| $N_L = 1$ | | | | |
| χ^2 | 1.79 | 1.70 | 1.43 | 1.42 |
| a_0 (nb/sr) | 88.1 ± 1.4 | 90.7 ± 1.5 | 92.3 ± 1.9 | 86.9 ± 1.2 |
| a_1 (nb/sr) | 25.8 ± 2.8 | 28.6 ± 2.9 | 28.3 ± 3.6 | 25.2 ± 2.4 |
| $N_L = 2$ | | | | |
| χ^2 | 1.58 | 1.39 | 1.39 | 1.27 |
| a_0 (nb/sr) | 88.9 ± 1.5 | 91.7 ± 1.6 | 92.9 ± 1.9 | 88.1 ± 1.3 |
| a_1 (nb/sr) | 26.8 ± 2.8 | 29.9 ± 2.9 | 28.4 ± 3.6 | 27.0 ± 2.4 |
| a_2 (nb/sr) | 9.7 ± 3.7 | 11.8 ± 3.9 | 7.1 ± 4.6 | 11.5 ± 3.2 |

tion by a_2 . In all cases, no significant improvements were obtained by expanding beyond $N_L = 2$.

Table II illustrates the results of the analysis using different coincidence conditions plus the full fit. One finds that the different analyses yield results in good agreement with one another, thereby providing a significant check on the consistency of the analysis procedure.

Table III summarizes the final results of the analysis. The uncertainties in the table include all but an estimated 10% uncertainty in the overall absolute normalization of the coefficients, which arises primarily from uncertainties in the π^0 tagging efficiency (5%), in the deuterium content of the targets (5%), and in the charge collection of the special Faraday cup (5%). All effects influencing the relative uncertainties of the parameters are incorporated in the values tabulated.

The differential cross sections resulting from this final analysis are illustrated in Fig. 6. The dashed lines indi-

cate the one sigma bounds of uncertainty. One observes that the cross sections depart rapidly from isotropy as one moves above threshold. The ratio of forward to backward cross sections is 1.9:1 at $T_{\pi}^{c.m.} = 0.11$ MeV, increasing to 6.8:1 at 2.68 MeV. The differential cross sections are fairly well described by a straight line when plotted as a function of $\cos\theta$, exhibiting a slight amount of curvature only at the two highest energies.

The analyzing powers, A_y , resulting from this analysis are illustrated in Fig. 7. This observable, following the Basel convention, is seen to be small and negative. Evidence for a significant contribution by b_2 was found only at the highest energy ($\eta = 0.20$).

The Legendre coefficients, a_l and b_l , resulting from the full analysis are tabulated in Table III and illustrated in Figs. 8 and 9 as functions of η , where $\eta \equiv p_{\pi}^{c.m.} / m_{\pi}c$. The curves drawn through the points have the momentum dependence η^{l+1} expected from "phase space" and are normalized to the data.

TABLE III. Summary of the results of the final analysis. The uncertainties quoted for a_l , b_l , and σ_{tot} do not include a 10% uncertainty in the absolute normalization.

| Parameter | Data set | | | |
|--|---------------------|---------------------|---------------------|---------------------|
| | Set 1 | Set 2 | Set 3 | Set 4 |
| T_p (MeV) | 198.91 ± 0.05 | 199.48 ± 0.04 | 201.06 ± 0.08 | 203.14 ± 0.10 |
| $T_{\pi}^{c.m.}$ (MeV) | 0.115 ± 0.030 | 0.461 ± 0.024 | 1.421 ± 0.049 | 2.684 ± 0.061 |
| $p_{\pi}^{c.m.}$ (MeV/c) | 5.57 ± 0.78 | 11.17 ± 0.30 | 19.64 ± 0.34 | 27.05 ± 0.31 |
| η | 0.0412 ± 0.0058 | 0.0827 ± 0.0022 | 0.1455 ± 0.0025 | 0.2004 ± 0.0023 |
| a_0 (nb/sr) | 41.0 ± 1.9 | 88.0 ± 2.5 | 145.0 ± 3.3 | 189.0 ± 5.5 |
| a_1 (nb/sr) | 11.0 ± 3.3 | 26.0 ± 3.0 | 90.0 ± 3.2 | 157.0 ± 5.0 |
| a_2 (nb/sr) | | | 12.0 ± 10.3 | 27.0 ± 10.0 |
| b_1 (nb/sr) | | 7.0 ± 3.0 | 15.0 ± 3.1 | 21.0 ± 4.0 |
| b_2 (nb/sr) | | | | 7.0 ± 4.6 |
| σ_{tot} (μb) | 0.515 ± 0.024 | 1.106 ± 0.031 | 1.822 ± 0.042 | 2.375 ± 0.069 |
| σ_{tot}/η (μb) | 12.50 ± 1.85 | 13.37 ± 0.52 | 12.52 ± 0.36 | 11.85 ± 0.37 |

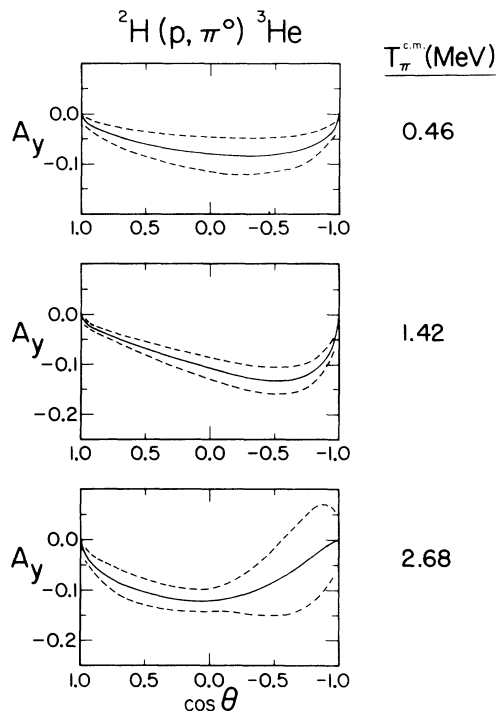


FIG. 7. Illustration of the analyzing powers resulting from the full analysis. The dashed lines indicate the one sigma bounds of uncertainty.

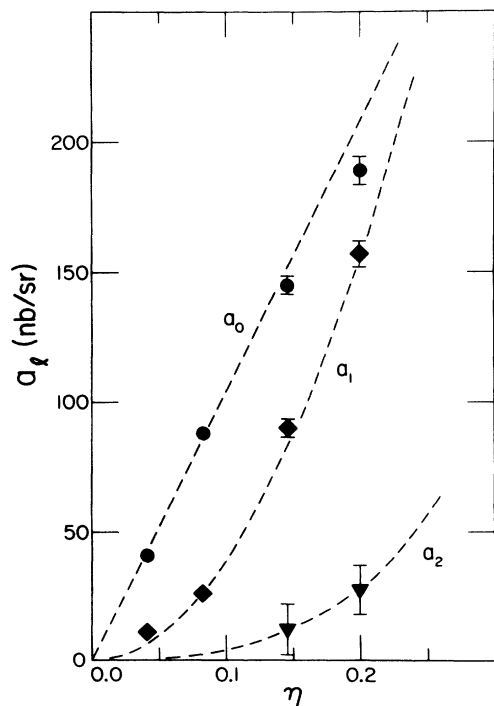


FIG. 8. Momentum dependence of the coefficients a_l resulting from a full fit to all the data. The dashed curves have the form η^{l+1} , and are normalized to the data. Solid circles are the results for a_0 , solid diamonds are the results for a_1 , and upside-down solid triangles are the results for a_2 .

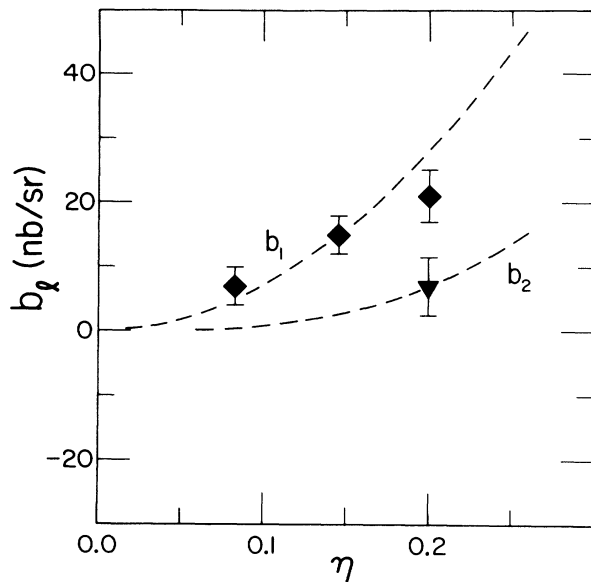


FIG. 9. Momentum dependence of the coefficients b_l resulting from a full fit to all the data. The dashed curves have the form η^{l+1} , and are normalized to the data. Solid diamonds are the results for b_1 , and upside-down closed triangles are the results for b_2 .

V. DISCUSSION

A. The low energy s -wave strength

If the energy dependence of a reaction near threshold is primarily determined by the density of final states (or, informally, “phase space”), then one expects, for $\eta \ll 1$, where η is the momentum of the light particle divided by its mass, that the amplitude for outgoing orbital angular momentum l is proportional to $\eta^{l+1/2}$. Unless the intrinsic strength for the different outgoing l values increases rapidly with increasing l (and we would not expect it to in this case, since $k_\pi R_{3\text{He}} < 0.25$), then the η dependence of the coefficients a_l and b_l of the Legendre expansion is $a_l \propto \eta^{l+1}$, $b_l \propto \eta^{l+1}$. The curves drawn in Figs. 8 and 9 loosely exhibit this expected dependence. The data are in general agreement with this expectation, although by $\eta=0.2$ the expected values of a_0 and perhaps b_1 fall somewhat below the curves.

However, the same model also leads one to expect $|a_{l+1}| \ll |a_l|$ and $|b_{l+1}| \ll |b_l|$. This behavior is seen in the present data for the lowest pion energies, but by $\eta=0.2$ ($T_\pi^{\text{c.m.}} = 2.7$ MeV) the coefficient a_1 is nearly equal to a_0 . Thus one cannot assume simply that because the pion energy is “small,” s -wave emission must dominate, and that one can find its energy dependence from the variation of a_0 . A more sophisticated approach is required.

If one examines the manner in which the Legendre coefficients a_l and b_l are related to the transition amplitudes for the reaction [4], one finds that a_0 is an incoherent sum of the squares of the transition amplitudes, and is related to the total cross section by $\sigma_{\text{tot}} = 4\pi a_0$. If

we restrict the discussion to s -, p -, and d -wave emission, the coefficients a_1 and b_1 arise from s - p and p - d wave interference. The coefficients a_2 and b_2 arise from p - p , s - d , and d - d wave interference. The increasing size of those coefficients a_l and b_l with $l > 0$ provides evidence for the increasing role of pions emitted with orbital angular momenta $l > 0$.

As we have noted, a_0 is the incoherent sum of the transition amplitudes. One may schematically write

$$\frac{1}{4\pi}\sigma_{\text{tot}} = a_0 = c_0|s|^2 + c_1|p|^2 + c_2|d|^2 + \dots, \quad (15)$$

where $c_l \geq 0$. If the momentum dependence of each amplitude is determined by "phase space," one expects

$$a_0 = d_0\eta + d_1\eta^3 + d_2\eta^5 + \dots \quad (16)$$

where $\eta \equiv p_\pi/m_\pi c$, and $d_l \geq 0$ for all l . Thus, one expects a_0 to vary linearly with η in that low energy region where s -wave emission dominates, and that it will begin to curve *upwards* and *away* from that line as higher order partial waves begin to contribute.

Upon examining Fig. 8, however, one finds that the coefficient a_0 does not exhibit this momentum dependence. As higher order partial waves contribute more and more at higher energies, as indicated by the increasing size of coefficients other than a_0 , one finds that a_0 curves *down* from the expected line proportional to η . One must conclude that the momentum dependence for this reaction begins to fall below the "phase space" expectation at energies as low as $T_\pi^{\text{c.m.}} \sim 1.5$ MeV.

In order to obtain a more quantitative measure of the s -wave strength, it is necessary to examine more closely the connection between the extracted Legendre coefficients and the transition amplitudes [4]. The complexity in the spin combination for the reaction ($\frac{1}{2}^+ + 1^+ \rightarrow \frac{1}{2}^+ + 0^-$) precludes the possibility of any unique determination of the amplitudes at any energy with data only for cross sections and analyzing powers. If one makes the assumption that only s - and p -wave emission are significant very close to threshold, one finds that one must determine seven amplitudes; two s -wave and five p -wave amplitudes. Thus a solution requires the determination of 13 parameters (given one arbitrary phase). Since only five parameters ($a_0, a_1, a_2, b_1,$ and b_2) could be extracted, and they are not independent, it is clear that even with increased precision a unique solution cannot be determined.

Lacking the possibility of obtaining a unique solution, various classes of solutions were examined. The classes are best differentiated by the degree of constructive interference between the partial waves. One finds in general that the greater the degree of constructive interference, the smaller the amount of p -wave strength required to reproduce the large asymmetry observed in the data.

In Fig. 10 are illustrated results of this study. The solid curve represents a linear fit to the measured momentum dependence of σ_{tot}/η . If the reaction yields only s -wave emission, and its momentum dependence is determined by "phase space," one expects σ_{tot}/η to be a constant. As higher order partial waves begin to contrib-

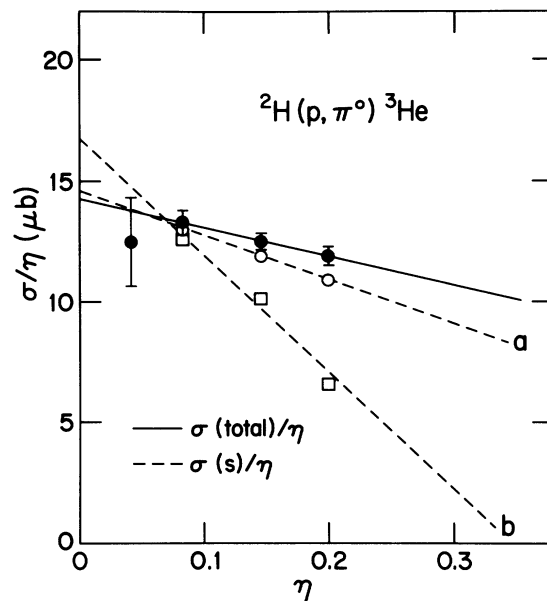


FIG. 10. Momentum dependence of the total cross sections for $pd \rightarrow {}^3\text{He}\pi^0$ measured near threshold (solid circles and solid line). The extracted s -wave strengths (open symbols and dashed lines) are those associated with the bounding solutions discussed in the text. Solution a , given by the open circles, is that with the *maximum* possible s -wave strength permitted by the data. Solution b , given by the open squares, is that with the *minimum* s -wave strength permitted by the data.

ute, this quantity should increase with η . The data, however, show a significant decrease with increasing η .

The dashed curves in Fig. 10 represent the fitted momentum dependence of the extracted s -wave strengths, as represented by $\sigma(s)/\eta$, for two bounding solutions. Curve b represents the approximate boundary for solutions requiring a minimum s -wave strength.

Curve a is significant in that it represents the results requiring the minimum p -wave strength needed to reproduce the data. It therefore represents the maximum s -wave strength permitted by the data.

There is some evidence that σ_{tot}/η decreases with η . After subtraction of the minimum possible p -wave strength, however, there is direct experimental evidence that the resulting momentum dependence of the maximum s -wave strength, $\sigma_{\text{max}}(s)/\eta$, deviates significantly from the phase space expectation at threshold.

All the results illustrated in Fig. 10 vary approximately linearly with η . If one parametrizes the s - and p -wave strengths with the functional forms

$$\sigma(s)/\eta = \alpha_0 + \alpha_1\eta, \quad (17)$$

$$\sigma(p)/\eta = \beta\eta^2, \quad (18)$$

giving a total cross section

$$\sigma_{\text{tot}}/\eta = \sigma(s)/\eta + \sigma(p)/\eta, \quad (19)$$

one obtains from all solutions values for α_1 that are significant and negative.

Because this study provides an estimate of the important role played by the α_1 term very near threshold, it

permits the extraction of $\sigma(s)/\eta$, and its uncertainty, at zero pion kinetic energy ($\eta=0$). This number is of great importance, because it can be directly compared to results from pionic atoms.

B. Comparison to results from pionic atoms

As in $pp \rightarrow d\pi^+$, there are symmetries connecting the reaction $pd \rightarrow {}^3\text{He}\pi^0$ at low pion energies to other processes. Of principal note are the interactions of stopped negative pions, π^- , in ${}^3\text{He}$. The branching fractions for various decay modes of such pions in ${}^3\text{He}$ have been measured by Zaimidoriga *et al.* [7,8], by Truöl *et al.* [9], and by Backenstoss *et al.* [10,11]. There have been two independent measurements of the shift and width of the pionic $1s$ level in liquid ${}^3\text{He}$ by Schwanner *et al.* [12,13], and by Mason *et al.* [14]. This information can be directly connected to the near threshold measurements for $pd \rightarrow {}^3\text{He}\pi^0$.

One recalls from the work of Deser, Goldberger, Baumann, and Thirring [15], and of Brueckner [16], that in the limit that the pion-nucleus strong interaction is short ranged and the pion atomic wave function varies little in the nuclear interior, the shift ϵ_{1s} and the width Γ_{1s} of the $1s$ atomic level can be related to the s -wave scattering length $a_{\pi A}$,

$$a_{\pi A} = -\frac{\mu_A}{2\pi\hbar^2\rho(0)}(\epsilon_{1s} - \frac{1}{2}i\Gamma_{1s}), \quad (20)$$

where μ_A is the pion-nucleus reduced mass and $\rho(0)$ is the probability density for the atomic pion at the origin. In the limit where only Coulomb effects are considered and the nucleus is treated as a point charge,

$$\rho(0) = \frac{1}{\pi}(Z\alpha\mu_A c/\hbar)^3. \quad (21)$$

This factor is modified by the extended charge of the nucleus and the strong interaction of the pion with the nucleus. Figereau and Ericson [17] estimate an approximately 4% decrease in the density of the pion atomic wave function in ${}^3\text{He}$ due to the extended charge of the nucleus, and an approximately 2% reduction due to the strong interaction.

Following arguments similar to those of Willis *et al.* [18], we next note that because at zero energy the only contribution to the imaginary part of the $\pi^- {}^3\text{He} \rightarrow \pi^- {}^3\text{He}$ amplitude must come from absorption alone, we obtain via the optical theorem,

$$\lim_{k_\pi \rightarrow 0} k_\pi \sigma(\pi^- {}^3\text{He} \rightarrow \text{absorption}) = 4\pi \text{Im}a_s. \quad (22)$$

Then, if the branching fraction for pions in a $1s$ atomic state to make the transition $\pi^- {}^3\text{He} \rightarrow nd$ is $B_d(s) = 0.137 \pm 0.016$ [11], we have

$$\lim_{k_\pi \rightarrow 0} k_\pi \sigma(\pi^- {}^3\text{He} \rightarrow nd) = 4\pi B_d(s) \text{Im}a_s. \quad (23)$$

We must next relate this to the reaction $pd \rightarrow {}^3\text{He}\pi^0$. Applying detailed balance and charge independence, and noting that p_n (the neutron momentum) is a very slowly varying function of k_π as $k_\pi \rightarrow 0$, we obtain

$$\begin{aligned} \lim_{\eta \rightarrow 0} \frac{1}{\eta} \sigma(pd \rightarrow {}^3\text{He}\pi^0) \\ = \frac{1}{6}(m_\pi/p_n^*)^2 \lim_{k_\pi \rightarrow 0} k_\pi \sigma(\pi^- {}^3\text{He} \rightarrow nd), \end{aligned} \quad (24)$$

where p_n^* is the $\lim_{k_\pi \rightarrow 0} p_n$.

If we now restrict the discussion to the s -wave strength, we obtain the final result

$$\begin{aligned} \lim_{\eta \rightarrow 0} \frac{1}{\eta} \sigma_s(pd \rightarrow {}^3\text{He}\pi^0) &= \frac{1}{6}(m_\pi/p_n^*)^2 4\pi B_d(s) \text{Im}a_s \\ &= 12.3 \pm 3.4 \mu\text{b} \quad [12,13] \\ &= 15.8 \pm 3.6 \mu\text{b} \quad [14] \\ &= 15.0 \pm 1.5 \mu\text{b} \quad (\text{this work}). \end{aligned} \quad (25)$$

We thus find good agreement between this experiment and the results of experimental studies of the $\pi^- {}^3\text{He}$ pionic atom. This lends substantial support to the accuracy of the procedures used in analyzing the $pd \rightarrow {}^3\text{He}\pi^0$ data and, in particular, to the absolute normalizations of the extracted cross sections.

The results of this work can also be directly related to the absorption rate for $1s$ negative pions in ${}^3\text{He}$ to the nd final state to give

$$\begin{aligned} W_{1s}(nd) &= \Gamma_{1s}(nd)/\hbar \\ &= (7.2 \pm 0.7) \times 10^{15} \text{ s}^{-1} \quad (\text{this work}). \end{aligned} \quad (26)$$

This quantity has also been calculated in a two-nucleon absorption model by several authors [17,19–21]. Phillips and Roig [21], who performed calculations using realistic nuclear wave functions and incorporated the effects of the nuclear short-range repulsion and the finite range of the pion absorption interaction, obtain $(8 \pm 2) \times 10^{15} \text{ s}^{-1}$ for $W_{1s}(nd)$ (see Table 3 of [21]).

Germond and Wilkin have expanded this approach and extended it to energies above threshold [22–24]. They are able to account for most known features of the reaction near threshold. They obtain the s -wave $\pi^- {}^3\text{He} \rightarrow nd$ branching ratio at rest in good agreement with data [23]. They also obtain tensor analyzing powers, t_{20} , in good agreement with data near threshold [23,24]. Their model accounts for the rapid departure from isotropy as one moves above threshold, and is in quantitative agreement with the results of this work [24]. However, their absolute cross sections are systematically smaller than the data [24].

C. Connection to higher energies

It is important to examine how the very low energy results obtained in this work match up with higher energy results. For $T_\pi^{\text{c.m.}} < 4 \text{ MeV}$ no other cross section data exist. In the important region between 4 and 44 MeV ($0.25 < \eta < 0.87$) the only existing data come from Saclay and consist only of 0° and 180° differential cross sections and tensor analyzing powers, t_{20} , for ${}^1\text{H}(\vec{d}, {}^3\text{He})\pi^0$ [25–27]. For $T_\pi^{\text{c.m.}} > 44 \text{ MeV}$ enough data exist to allow

one to extract total cross sections and shape parameters with good accuracy. This information, coupled with the low energy results of this work, permits one to determine total cross sections and the first order shape parameters from the 0° and 180° measurements from Saclay.

If the differential cross section is expanded in a Legendre series, as in Eq. (1), we may write the 0° and 180° cross sections as

$$d\sigma(0^\circ) = a_0 + a_1 + a_2 + a_3 + \dots, \quad (27)$$

$$d\sigma(180^\circ) = a_0 - a_1 + a_2 - a_3 + \dots.$$

We can then obtain expressions for a_0 and a_1 in terms of the measured cross sections and deduced shape parameters (a_i/a_0 and a_i/a_1):

$$a_0 = \frac{[d\sigma(0^\circ) + d\sigma(180^\circ)]/2}{1 + a_2/a_0 + a_4/a_0 + \dots}, \quad (28)$$

$$a_1 = \frac{[d\sigma(0^\circ) - d\sigma(180^\circ)]/2}{1 + a_3/a_1 + a_5/a_1 + \dots}. \quad (29)$$

The shape parameters in the denominators of the above two expressions were evaluated at $T_\pi^{\text{c.m.}}$ energies higher than 44 MeV by fitting available data for complete angular distributions [4,28–33]. Since these terms are small below 35 MeV, one is able to deduce their values with sufficient accuracy to permit determinations of a_0 and a_1 . At higher energies they can be obtained from the systematics of the high energy fits [4].

In Fig. 11 one sees the resulting momentum dependence of σ_{tot}/η for $pd \rightarrow {}^3\text{He}\pi^0$, where σ_{tot} is the total cross section, $4\pi a_0$. The error bars include contributions from uncertainties in the extraction procedure. The figure also includes total cross sections extracted from other data sets for which complete angular distributions are available [28,29,32,33].

It is apparent from Fig. 11 that there may exist significant differences in absolute normalization between the different data sets. There exist other data sets, from which total cross sections cannot be extracted, but which overlap the measurements represented in Fig. 11 in restricted angular regions. Of special note are comparisons to the low energy results of [32] (at $\eta=0.86, 1.29$) and [28] (at $\eta=1.20$). The results of [34] (at $\eta=0.98$ and 1.15 , for $\theta > 90^\circ$) are systematically larger than those of [32] by a factor of 2. They are larger than the results of [28] by a factor of 1.5. The results of [35] (at $\eta=1.00$ and 1.15 , for $\theta > 70^\circ$) are systematically larger than those of [32] and [28] by a factor of 2.

The data of [33] at $\eta=1.33$ were fit to a Legendre expansion. The resulting extracted differential cross section at 0° can be compared directly to the result of [25–27] at $\eta=1.33$, and is found to be a factor of 1.4 smaller (consistent with the difference between the extracted total cross sections seen in Fig. 11). One can also use the results of this work to extract the 0° differential cross section at $\eta=0.25$, and compare it directly to the result of [25–27] at $\eta=0.25$. It is found to be a factor of 1.5 lower than the result of [25–27], again consistent with the difference between the extracted total cross sections seen in Fig. 11.

Even with the problems of absolute normalization, it is clear that one of the most striking aspects of the resulting excitation function is the absence of a dramatic resonance-like feature of the type observed in $pn \rightarrow d\pi^0$, illustrated by the solid curve in Fig. 11 (note also that the cross sections for $pn \rightarrow d\pi^0$ have been divided by a factor of 40). One finds σ_{tot}/η for $pd \rightarrow {}^3\text{He}\pi^0$ to be relatively constant from $\eta=0$ (pionic atoms) up through $\eta=1.4$ ($T_\pi^{\text{c.m.}} \simeq 100$ MeV). There is only the trace of a small enhancement in the total cross section near $\eta=1$. This differs *greatly* from $pn \rightarrow d\pi^0$, for which σ_{tot}/η at threshold is ~ 11 times smaller than the value attained at the peak of the resonance.

Given the observed strong anisotropy of the differential cross section for $pd \rightarrow {}^3\text{He}\pi^0$ one knows that the total cross section must have significant contributions from partial waves other than s wave in this region. The fact that σ_{tot}/η is relatively constant indicates that the influence of form factor effects is significant. Thus, any model attempting to connect the very low energy data,

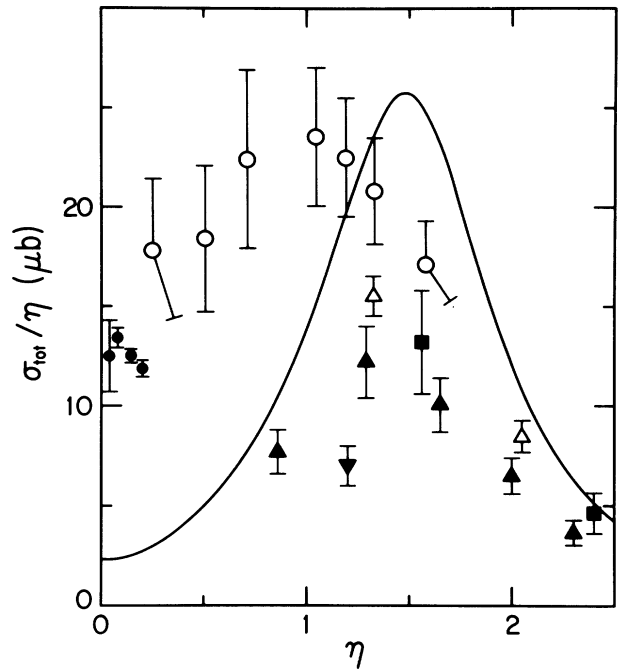


FIG. 11. Momentum dependence of σ_{tot}/η for $pd \rightarrow {}^3\text{He}\pi^0$ over an extended kinematic range. The solid circles are data from this work. The open circles are the extracted total cross sections from the data of [25–27]. The solid triangles are the extracted total cross sections from the data of [32]. The inverted solid triangle is the extracted total cross section from the data of [28]. The open triangles are the extracted total cross sections from the data of [33]. The solid squares are the extracted total cross sections from the data of [29]. The solid curve shows the momentum dependence of $\frac{1}{40} \times \sigma_{\text{tot}}/\eta$ for the fundamental reaction $pn \rightarrow d\pi^0$. The curve was generated for $\eta > 0.3$ using the functional form given by Ritchie [37], after application of detailed balance, charge independence, and Coulomb corrections [38]. For $\eta < 0.3$ the functional form given by Hutcheon *et al.* [36] was used.

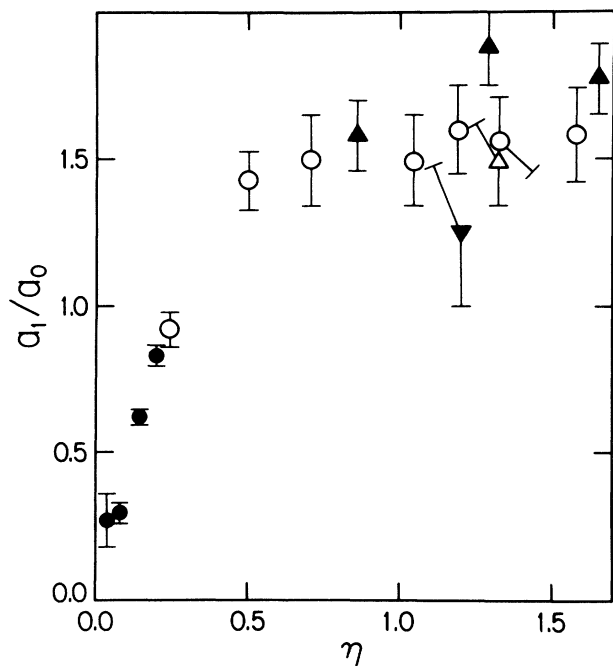


FIG. 12. Momentum dependence of the shape parameter a_1/a_0 for $pd \rightarrow {}^3\text{He}\pi^0$. The data are from the same sources described in Fig. 11.

obtained in this work, with the higher energy data must account for these effects.

In Fig. 12 are plotted the available data for the parameter a_1/a_0 . Examining the data in this way helps remove problems associated with uncertainties in the absolute normalization for the measured cross sections. One observes that this first order shape parameter changes smoothly with η as one goes to higher energies, and that irregularities of the size observed in the total cross section (Fig. 11) are absent.

VI. CONCLUSIONS

In this experiment the reaction $pd \rightarrow {}^3\text{He}\pi^0$ has been studied in a new kinematic region. Apart from studies of

pionic atoms, this region ($0.04 \leq \eta \leq 0.20$) is closer to threshold than *any* study of (N, π) , or (π, N) , from a multinucleon target. This work also provides the first data in the threshold region for exclusive production from deuterium, and hence serves as a bridge between pion production from the nucleon and pion production from heavy targets in that kinematic region.

The total cross sections resulting from this experiment are in good agreement with results extracted from studies of pionic atoms. These new data also make possible a significant comparison of the excitation function, σ/η , for $pn \rightarrow d\pi^0$ to that for $pd \rightarrow {}^3\text{He}\pi^0$ over a comprehensive range of pion momenta. We find that the addition of a single nucleon removes evidence of a dramatic resonance-like feature in this few-nucleon system of the type observed in the two-nucleon system. This is taken to be evidence for the important role of form factor effects.

The experiment yielded sufficient precision to examine, in the very-near-threshold region, the momentum dependence of the extracted Legendre coefficients a_0 , a_1 , and a_2 , describing the total and differential cross sections, and b_1 and b_2 , describing the spin-observable $A_y d\sigma/d\Omega$. This new information has made clear that, although s -wave pion emission from the nucleus dominates in this low energy region, pion emission involving higher order partial waves, most notably p waves, exhibits itself dramatically through interference terms. One finds that a_1 , which results principally from s - p wave interference in the threshold region, becomes nearly equal to a_0 by $\eta = 0.20$ ($T_\pi^{\text{c.m.}} = 2.7$ MeV).

This strong manifestation of the effects of p -wave emission near threshold motivated an attempt to make a more quantitative estimate of the relative strengths for s - and p -wave emission at such low energies. As a result of this exercise one finds that the momentum dependence of the s -wave strength is not adequately described by phase space alone. It is determined that the excitation function for the s -wave strength, $\sigma(s)/\eta$, decreases with η in this kinematic region, rather than being constant.

This work was supported in part by Grant No. PHY-9103794 from the U.S. National Science Foundation.

[1] R. D. Bent, D. G. Madland, J. D. Cossairt, A. D. Bacher, W. P. Jones, D. W. Miller, R. E. Pollock, and P. Schwandt, IUCF Int. Report No. 1-73, 1973.
 [2] *Indiana University Cyclotron Facility User's Manual*, compiled by G. T. Emery (IUCF, Bloomington, 1975).
 [3] *Indiana University Cyclotron Facility Technical and Scientific Report, Nov. 1, 1975–Jan. 31, 1977*, compiled by H. A. Smith, Jr., D. L. Friesel, and J. E. Thornburg (IUCF, Bloomington, 1977), p. 22.
 [4] M. A. Pickar, Ph.D. thesis, Indiana University, 1982.
 [5] M. A. Pickar, in *Pion Production and Absorption in Nuclei—1981 (Indiana University Cyclotron Facility)*, Proceedings of the Conference on Pion Production and Absorption in Nuclei, edited by R. D. Bent, AIP Conf. Proc. No. 79 (AIP, New York, 1982), p. 143.
 [6] M. Abramowitz and I. A. Stegun, *Handbook of Mathematical Functions* (Dover, New York, 1972), p. 334.

[7] O. A. Zaimidoroga, M. M. Kulyukin, R. M. Sulyaev, I. V. Falomkin, A. I. Filippov, V. M. Tsupko-Sitnikov, and Yu. A. Shcherbakov, *Zh. Eksp. Teor. Fiz.* **48**, 1267 (1965) [Sov. Phys. JETP **21**, 848 (1965)].
 [8] O. A. Zaimidoroga, M. M. Kulyukin, R. M. Sulyaev, I. V. Falomkin, A. I. Filippov, V. M. Tsupko-Sitnikov, and Yu. A. Shcherbakov, *Zh. Eksp. Teor. Fiz.* **51**, 1646 (1966) [Sov. Phys. JETP **24**, 1111 (1967)].
 [9] P. Truöl, H. W. Baer, J. A. Bistirlich, K. M. Crowe, N. de Botton, and J. A. Helland, *Phys. Rev. Lett.* **32**, 1268 (1974).
 [10] G. Backenstoss, W. Kowald, I. Schwanner, H.-J. Weyer, M. Dörr, D. Gotta, G. Schmidt, L. M. Simons, and H. Ullrich, *Phys. Lett.* **115B**, 445 (1983).
 [11] G. Backenstoss, M. Izycki, W. Kowald, P. Weber, H.-J. Weyer, S. Ljungfelt, U. Mankin, G. Schmidt, and H. Ullrich, *Nucl. Phys.* **A448**, 567 (1986).

- [12] I. Schwanner, R. Abela, G. Backenstoss, W. Kowald, P. Pavlopoulos, L. Tauscher, H.-J. Weyer, P. Blüm, M. Dörr, W. Fetscher, D. Gotta, R. Guigas, H. Koch, H. Poth, G. Schmidt, and H. Ullrich, *Phys. Lett.* **96B**, 268 (1980).
- [13] I. Schwanner, G. Backenstoss, W. Kowald, L. Tauscher, H.-J. Weyer, D. Gotta, and H. Ullrich, *Nucl. Phys.* **A412**, 253 (1984).
- [14] G. R. Mason, G. A. Beer, M. S. Dixit, S. K. Kim, J. A. MacDonald, A. Olin, R. M. Pearce, W. C. Sperry, and J. S. Vincent, *Nucl. Phys.* **A340**, 240 (1980).
- [15] S. Deser, M. C. Goldberger, K. Baumann, and W. Thirring, *Phys. Rev.* **96**, 774 (1954).
- [16] K. A. Brueckner, *Phys. Rev.* **98**, 769 (1955).
- [17] A. Figureau and M. Ericson, *Nucl. Phys.* **B10**, 349 (1969).
- [18] N. Willis, L. Bimbot, N. Koori, Y. Le Bornec, F. Reide, A. Willis, and C. Wilkin, *J. Phys. G* **7**, L195 (1981).
- [19] P. P. Divakaran, *Phys. Rev.* **139**, B387 (1965).
- [20] C. Pajares and R. Pascual, *Nucl. Phys.* **B35**, 631 (1971).
- [21] A. C. Phillips and F. Roig, *Nucl. Phys.* **B60**, 93 (1973).
- [22] J.-F. Germond and C. Wilkin, *J. Phys. G* **12**, 1379 (1986).
- [23] J.-F. Germond and C. Wilkin, *J. Phys. G* **14**, 181 (1988).
- [24] J.-F. Germond and C. Wilkin, *J. Phys. G* **16**, 381 (1990).
- [25] C. Kerboul, A. Boudard, L. Antonuk, J. Arvieux, J. Berger, R. Bertini, M. Boivin, J. M. Durand, A. Stetz, J. Tinsley, J. Yonnet, Nguyen Van Sen, Ye Yanlin, B. Mayer, J. Cameron, C. Lapointe, D. M. Sheppard, J. F. Germond, and C. Wilkin, *Phys. Lett. B* **181**, 28 (1986).
- [26] A. Boudard, C. Kerboul, L. Antonuk, J. Arvieux, J. Berger, R. Bertini, M. Boivin, J. M. Durand, G. Roy, J. Tinsley, J. Yonnet, B. Mayer, and Nguyen Van Sen, *Phys. Lett. B* **214**, 6 (1988).
- [27] F. Plouin, in *Production and Decay of Light Mesons*, edited by P. Fleury (World Scientific, Singapore, 1988), p. 114.
- [28] W. J. Frank, K. C. Bandtel, R. Madey, and B. J. Moyer, *Phys. Rev.* **94**, 1716 (1954).
- [29] E. Aslanides, R. Bertini, O. Bing, F. Brochard, Ph. Gorodetzky, F. Hibou, T. S. Bauer, R. Beurtey, A. Boudard, G. Bruge, G. Catz, A. Chaumeaux, P. Couvert, H. H. Duhm, D. Garreta, G. Igo, J. C. Lugol, M. Matoba, Y. Terrien, L. Bimbot, Y. Le Bornec, and B. Tatischeff, *Phys. Rev. Lett.* **39**, 1654 (1977).
- [30] L. Orphanos, J. Källne, R. Altemus, P. C. Gugelot, J. S. McCarthy, R. C. Minehart, P. A. M. Gram, B. Höistad, C. L. Morris, E. A. Wadlinger, and C. Perdrisat, *Phys. Rev. Lett.* **46**, 1562 (1981).
- [31] J. M. Cameron, L. G. Greeniaus, D. A. Hutcheon, C. A. Miller, G. A. Moss, R. P. Liljestrang, H. Wilson, R. Abegg, W. T. H. van Oers, A. W. Stetz, M. B. Epstein, and D. J. Margaziotis, *Phys. Lett.* **103B**, 317 (1981).
- [32] J. Källne, J. E. Bolger, M. J. Devereaux, and S. Z. Verbeck, *Phys. Rev. C* **24**, 1102 (1981).
- [33] J. M. Cameron, P. Kitching, J. Pasos, J. Thekkumthala, R. Abegg, D. A. Hutcheon, C. A. Miller, S. A. Elbakr, and A. H. Hussein, *Nucl. Phys.* **A472**, 718 (1987).
- [34] K. A. Aniol, A. Altman, R. R. Johnson, H. W. Roser, R. Tacik, U. Wienands, D. Ashery, J. Alster, M. A. Moines-ter, E. Piassetzky, D. R. Gill, and J. Vincent, *Phys. Rev. C* **33**, 1714 (1986).
- [35] G. J. Lolos, E. L. Mathie, G. Jones, E. G. Auld, G. Giles, B. McFarland, P. L. Walden, W. Ziegler, and W. R. Falk, *Nucl. Phys.* **A386**, 477 (1982).
- [36] D. A. Hutcheon, E. Korkmaz, G. A. Moss, R. Abegg, N. E. Davison, G. W. R. Edwards, L. G. Greeniaus, D. Mack, C. A. Miller, W. C. Olsen, I. J. van Heerden, and Ye Yanlin, *Phys. Rev. Lett.* **64**, 176 (1990).
- [37] B. G. Ritchie, *Phys. Rev. C* **44**, 533 (1991).
- [38] A. Reitan, *Nucl. Phys.* **B11**, 170 (1969).